

Where are the missing baryons in clusters?

Bilhuda Rasheed, Neta Bahcall, and Paul Bode
*Department of Astrophysical Sciences, 4 Ivy Lane,
Pepton Hall, Princeton University, Princeton, NJ 08544*

Observations of clusters of galaxies suggest that they contain significantly fewer baryons (gas plus stars) than the cosmic baryon fraction. This ‘missing baryon’ puzzle is especially surprising for the most massive clusters which are expected to be representative of the cosmic matter content of the universe (baryons and dark matter). Here we show that the baryons may not actually be missing from clusters, but rather are extended to larger radii than typically observed. The baryon deficiency is typically observed in the central regions of clusters (~ 0.5 the virial radius). However, the observed gas-density profile is significantly shallower than the mass-density profile, implying that the gas is more extended than the mass and that the gas fraction increases with radius. We use the observed density profiles of gas and mass in clusters to extrapolate the measured baryon fraction as a function of radius and as a function of cluster mass. We find that the baryon fraction reaches the cosmic value near the virial radius for all groups and clusters above $\sim 5 \times 10^{13} h_{72}^{-1} M_{\odot}$. This suggests that the baryons are not missing, they are simply located in cluster outskirts. Heating processes (shock-heating of the intracluster gas, plus supernovae and AGN feedback) that cause the gas to expand are likely explanations for these results. Upcoming observations should be able to detect these baryons.

I. INTRODUCTION

Clusters of galaxies, the largest virialized systems in the universe, are powerful tools in constraining cosmology and tracing the large-scale structure of the universe [1–4, and references therein]. The large mass of clusters ($\sim 10^{14}$ to $10^{15} h_{72}^{-1} M_{\odot}$) implies that their contents—dark and baryonic matter—have been accreted from very large regions of ~ 10 comoving Mpc, and therefore should be representative of the mean matter content of the universe. The strong gravitational potential of clusters also implies that baryons cannot easily escape from these systems. Therefore, clusters are expected to retain the cosmic baryon fraction, i.e., the relative fraction of baryons to total matter. This basic assumption of a representative baryon fraction in clusters was used in 1993 [5] to suggest that the mass-density of the universe must be low, since the observed baryon fraction in clusters was considerably larger than expected for a critical density universe. Most of the baryons in clusters reside in the X-ray emitting hot intracluster gas, which approximately traces the cluster gravitational potential dominated by dark matter. The rest of the baryons are in the luminous galaxies and in isolated stars that comprise the small amount of faint diffuse intracluster light (ICL).

A puzzle has been raised, however, over the last few years: Detailed X-ray observations from *Chandra*, *XMM-Newton* and others suggest that the cluster baryon fraction (gas plus stars relative to total mass) is considerably lower than the cosmic value [6–11]. The cosmic baryon fraction is well determined both from Big-Bang nucleosynthesis [12, 13] and from observations of the Cosmic Microwave Background to be $f_b = 0.1675 \pm 0.006$ [WMAP7: 14]. The cluster gas fraction has been reported by the above observations to be only 60 – 80% of the cosmic value, with stars contributing only a small ($\sim 10\%$) additional amount of baryons. This baryon dis-

crepancy is observed to increase with decreasing cluster mass [10, 11]. This raises the questions: Where are the missing baryons? Why are they ‘missing’?

Attempted explanations for the missing baryons in clusters range from preheating or other energy inputs which expel gas from the system [15–21, and references therein], to the suggestion of additional baryonic components not yet detected [e.g., cool gas, faint stars 6, 22].

In this paper we investigate the possibility that the ‘missing baryons’ are not missing at all, but are rather located in the outskirts of clusters where few detailed observations have yet been made. The ‘missing baryons’ problem is typically observed within the central regions of clusters, generally within a radius of R_{500} (where the enclosed mass-density is 500 times the critical density). This radius is ~ 0.5 of the virial radius of the cluster (where the enclosed density is ~ 100 times the critical density, for the current LCDM cosmology [23, 24]). Thus for a virial radius of ~ 1.5 Mpc, the typical missing baryon problem is observed only at ~ 0.75 Mpc from the cluster center.

Observations show that the gas density profile in the outer parts of clusters decreases with radius slower than the mass profile in these regions. Using gravitational lensing, the latter has been observed out to large radii [7, 38, 39] and is consistent with the expected NFW profile [25]. While the cluster mass-density declines with radius approximately as $r^{-2.6}$ in these outer regions, the gas-density declines only as $r^{-2.2}$. This implies that the gas is more extended than the total mass, and therefore the gas fraction increases with radius beyond the observed radius of R_{500} . A shallow slope of the gas profile (as compared with the mass profile) is indeed expected if gas heating occurs in the clusters (e.g., from shock-heating of the gas, supernovae, and AGNs; these processes are known to exist). The heating expands the gas relative to the dark matter potential and spreads it out to larger

radii, with a shallower slope, as observed.

We use the observed slopes of the gas-density and mass-density profiles in the outer regions of clusters to extrapolate the observed gas fraction from R_{500} to larger radii, up to the virial radius ($R_{vir} = R_{100}$ [23, 24]). We add the observed stellar fraction to the extrapolated gas fraction to find the baryon fraction at large radii. We perform this extrapolation as a function of cluster mass, from groups to rich clusters. Our analysis is based entirely on observations.

We find that there is no ‘missing baryon’ problem in rich clusters when the data is extrapolated to near the virial radius; at that radius, the baryon fraction is consistent with the cosmic value. Most of the ‘missing baryons’ are therefore expected to be in the outskirts of clusters, between R_{500} and R_{vir} . This result can be tested with upcoming observations of the Sunyaev-Zeldovich effect in clusters (e.g., SPT [27]; ACT [26]) as well as with more sensitive X-ray observations.

Observations have shown that the ‘missing baryon’ problem at R_{500} becomes significantly more severe for lower mass clusters and groups of galaxies than for rich clusters; the observed gas fraction decreases considerably with decreasing cluster mass. This too would be expected if the heating processes expand the gas: the lower gravitational potential of the smaller systems will not be able to hold on to their gas as well as the higher mass clusters. The gas density profile in small groups is indeed observed to be shallower than the gas density profile in massive clusters, suggesting that the gas in low mass systems is more spread out. We extrapolate the observed baryon fraction as described above for clusters as a function of their mass—from groups to rich clusters. We find that for this entire mass range the baryon fraction within R_{vir} is flat and is consistent with the cosmic value.

In the next section we describe the observations and analysis. A discussion of the results and our conclusions follow. We use a LCDM cosmology with $h=0.72$ and $\Omega_m=0.258$.

II. OBSERVATIONS, ANALYSIS AND RESULTS

The gas fraction in clusters of galaxies has been measured for a relatively large sample of groups and clusters within R_{500} . The total baryon fraction is obtained by adding the stellar mass fraction observed for these systems within the same radius. This baryon fraction is systematically lower than the cosmic value measured by WMAP7; the discrepancy increases with decreasing cluster mass [10, 11, and references therein]. Here we investigate the possibility that the missing baryons are not actually missing from clusters but are rather spread out to larger radii, beyond R_{500} . We investigate this scenario by extrapolating the observed gas fraction to larger radii, from R_{500} up to the virial radius ($R_{vir} = R_{100}$), using the mean observed gas and mass density profiles in clusters; these density profiles have been measured up to the virial

radius (and occasionally beyond). The observed stellar mass fraction, including the small contribution from the ICL, is added to the gas fraction to yield the total baryon fraction. The baryon fraction is then investigated as a function of radius, from R_{500} to R_{vir} , and as a function of mass, from groups to rich clusters.

A. Gas Fraction at R_{500}

Although some observations extend to R_{200} , the gas fraction has been accurately measured for a sufficiently large sample of nearby clusters only out to R_{500} .

We use X-ray observations of the gas fractions for 39 nearby clusters observed with *Chandra* and *XMM-Newton* [8–10]. These authors use similar methods of data reduction and analysis. We use the compilation by Giodini et al. [11] of these groups and clusters above the mass of $M_{500} = 3 \times 10^{13} h_{72}^{-1} M_{\odot}$ (where M_{500} is the mass within R_{500}). After conversion to a common cosmology (LCDM with $\Omega_m = 0.258$ and $H_0 = 72$ km/s/Mpc), the three samples have been binned into four logarithmically spaced mass bins, from groups to rich clusters [11]. (We do not include the lowest mass bin at $10^{13} h_{72}^{-1} M_{\odot}$ which contains only two groups with large error bars.) Our cluster sample has a mass range of $3 \times 10^{13} h_{72}^{-1} M_{\odot} < M_{500} < 10^{15} h_{72}^{-1} M_{\odot}$ and a redshift range of $0.012 < z < 0.23$. The mean observed gas fraction for each mass bin is listed in Table 1 and shown in Figure 1. The error on the mean is the rms standard deviation divided by $\sqrt{N-1}$. The horizontal bars are the mass ranges for the bins. Also presented in Figure 1 is the cosmic baryon fraction observed by the WMAP7 microwave background measurements, $f_b = 0.1675 \pm 0.006$ [14]. One can see that the cluster gas fraction at R_{500} is significantly lower than the cosmic baryon fraction. The gas fraction decreases significantly from rich to poor clusters; while rich clusters contain about 12% gas within R_{500} , the gas fraction in poor clusters and groups is only ~ 6 -7%.

B. Stellar Fraction

The galactic stellar fraction has been measured in nearby clusters using multiband optical and infrared surveys combined with stellar population models. We use the results obtained from the COSMOS survey [11] and 2MASS survey [28] for nearby clusters. The combined COSMOS and 2MASS sample covers our entire cluster mass range, $3 \times 10^{13} - 10^{15} h_{72}^{-1} M_{\odot}$. We bin the observed stellar fraction into the same four logarithmic mass bins as the gas fraction sample. The mean stellar fraction declines with cluster mass as $M^{-0.37 \pm 0.04}$ [see 11, Figure 5], exhibiting an opposite trend to that of the gas fraction.

To determine the contribution of the diffuse intracluster light (ICL) to the stellar fraction, we use the observations by Zibetti [29] which use the Sloan Digital Sky

TABLE I: Cluster gas, stellar, and total baryon fractions within R_{500}

Bin	$\langle M_{500} \rangle$ ($h_{72}^{-1} M_{\odot}$)	f_{500}^{gas}	$f_{500}^{stars+ICL}$	f_{500}^b
1	5.1×10^{13}	0.068 ± 0.005	0.050 ± 0.002	0.118 ± 0.005
2	1.2×10^{14}	0.080 ± 0.003	0.040 ± 0.004	0.120 ± 0.005
3	3.0×10^{14}	0.103 ± 0.008	0.023 ± 0.002	0.126 ± 0.009
4	7.1×10^{14}	0.123 ± 0.007	0.021 ± 0.002	0.143 ± 0.007

Gas, stellar (including ICL), and baryon fraction of clusters within R_{500} for four cluster mass bins: Bin 1 ($0.3 - 0.7 \times 10^{14} h_{72}^{-1} M_{\odot}$), Bin 2 ($0.7 - 1.7 \times 10^{14} h_{72}^{-1} M_{\odot}$), Bin 3 ($1.7 - 4.2 \times 10^{14} h_{72}^{-1} M_{\odot}$) and Bin 4 ($4.2 - 10 \times 10^{14} h_{72}^{-1} M_{\odot}$). f_{500}^{gas} are averages from Chandra and XMM observations [8–11]. f_{500}^{stars} and the 10% ICL contribution are from [11, 28, 29]. The error bars are 1- σ errors on the mean.

Survey data to reach to unprecedented cluster-centric distances and depth for a large number of stacked clusters of various masses. They find the ICL is centrally concentrated, and that on average the ICL contributes $\sim 10\%$ of the stellar light within the central 500 kpc for all cluster masses. We add this 10% contribution to the galactic stellar fraction discussed above for all clusters. We note that the ICL contribution may decline to less than 10% when extending to larger cluster radii; but since the ICL is a very small contribution to the total baryon fraction, this effect has negligible consequences (see Discussion). The total stellar fraction for the four mass bins is summarized in Table 1. It is added to the gas fraction to obtain the total average baryon fraction for each mass range. The baryon fraction within R_{500} is listed in Table 1 and plotted as a function of mass in Figure 1. The deficiency of baryons within R_{500} relative to the cosmic value is clearly seen in Figure 1; the deficiency becomes more severe for lower mass clusters.

C. Gas and Mass Density Profiles

Extrapolating the observed gas fraction to larger radii beyond R_{500} requires the knowledge of the observed gas and mass density profiles in these regions. The gas density profile has been measured well in the outer parts of clusters ($R_{500} - R_{vir}$) using X-ray observations of nearby clusters with *ROSAT*, *Chandra*, *XMM-Newton*, and *Suzaku*. The observed gas profile in the outer regions fits well to a beta-model with a density slope of $3\beta_{gas} = \alpha_{gas}$ (where $\rho_{gas} \propto r^{-\alpha_{gas}}$). We use observations with small uncertainties on the gas density slope at large radii and which cover our entire cluster mass range [8, 31–34].

The averaged observed β -values of the gas density slope are presented as a function of cluster temperature in Fig-

ure 2. The data include measurements for 51 clusters as well as average slopes for stacked samples of hundreds of optical clusters; the slopes are binned in temperature as presented in Figure 2. The error bars on the bin-averaged gas slopes are the standard deviation divided by $\sqrt{N-1}$. The *ROSAT* observations of 39 $z < 0.25$ clusters by Vikhlinin et al. [31] cover the full outer regions of clusters, from $0.3R_{500}$ to $1.5R_{180}$ ($\sim R_{vir}$). The best-fit slope to these outer regions is determined for a wide range of cluster temperature, from 2 keV to over 10 keV. The *Chandra* observations of 10 massive clusters by Vikhlinin et al. [8] provide β -fits to gas density slopes near R_{500} , nicely consistent with the trend shown by the slopes of the previous sample [31]. For the lowest mass bin ($M_{500} \approx 5 \times 10^{13} h_{72}^{-1} M_{\odot}$) we use the observed density slope from *ROSAT* by Dai et al. [32, their richness class 1], who obtain integrated X-ray gas profile for stacked samples of hundreds of low-mass optical clusters out to R_{vir} . We also include Bautz et al. [33] who measure the gas profile of Abell 1745 to R_{200} using *Suzaku* observations.

The observed beta slopes presented in Figure 2 are consistent with each other, and show a shallower slope for lower mass systems than for massive clusters. For our four mass bins (Table 1, Figure 1) we find the following mean gas density slopes: $\alpha_{gas} = 3 \times \beta_{gas} = 1.8 \pm 0.2$ for Bin 1, 1.9 ± 0.07 for Bin 2, 2.1 ± 0.02 for Bin 3, and 2.3 ± 0.02 for Bin 4. The error bars are the standard deviation of the average β -values in each bin divided by $\sqrt{N-1}$. When comparing a slope at a given temperature bin in Figure 2 to a given mass bin in Figure 1, we use the observed $M_{500} - T$ relation [8]; the results are not sensitive to the exact conversion because of the slowly varying $\beta_{gas}(T)$ relation.

The final piece required for extrapolating the gas (and baryon) fraction to large radii is the total mass density profile. This has been observed to follow the NFW profile [25] to large radii, by using weak lensing observations with the Sloan Digital Sky Survey and other observations [7, 38, 39, and references therein]. We use the average observed value of the concentration parameter $c_{200} = 5$ for our mass range [38]. The NFW profile has a mass density slope of $\alpha_m = 2.6$ in the radius range from R_{500} to R_{200} , and $\alpha_m = 2.7$ from R_{200} to R_{vir} (where $\rho_m \propto r^{-\alpha_m}$). These slopes are considerably steeper than the corresponding gas density slopes, thus yielding an increasing gas fraction with radius in cluster outskirts.

D. Extrapolation and Results

Using the observed gas density and mass density slopes at large radii, we extrapolate the observed gas fraction from R_{500} as a function of radius up to the virial radius. The gas fraction increases with radius as:

$$f^{gas}(< R) \propto \frac{\rho_{gas}(R) \propto R^{-\alpha_{gas}}}{\rho_m(R) \propto R^{-\alpha_m}} \propto R^{\alpha_m - \alpha_{gas}}, \quad r > R_{500}.$$

The extrapolated gas fraction from R_{500} to R_{200} and to R_{vir} is presented as a function of cluster mass in Figure 3a. Because the gas density slope is shallower in groups than in rich clusters, the increasing trend of gas fraction with mass becomes weaker at the outer radii.

The baryon fraction is presented for the different radii— R_{500} , R_{200} , and R_{vir} —as a function of mass in Figure 3b; the baryon fraction within these radii is the sum of the gas fraction (Figure 3a) and the stellar mass fraction discussed above, including the 10% ICL. We assume that this fraction remains constant with increasing radius; the main results do not change significantly if this assumption is changed because of the relatively small contribution of the stellar component (see Discussion). The error bar on the extrapolated gas fraction is the propagated errors of the gas fraction at R_{500} and the gas slope used for extrapolation. The error bar on the baryon fraction is the combined errors of the gas and stellar fractions.

The results in Figure 3b show that the baryon fraction flattens considerably as a function of cluster mass when extrapolated to larger radii; this is due to the combined effect of the shallower gas density profile in groups, which results in more gas in their outskirts, plus the larger observed stellar mass fraction in groups, which adds more baryons in the smaller systems. In fact, at the virial radius we find that the baryon fraction is essentially flat from groups to rich clusters, at a level consistent with the cosmic baryon fraction. This suggests that there are no ‘missing baryons’: most of the ‘missing baryons’ are likely located in the outskirts of clusters, extending to nearly the virial radius.

The extrapolated baryon fraction is presented as a function of radius for two of our mass bins (Bins 2 and 4) in Figure 4; the results show the slow but steady increase in the baryon fraction with radius.

III. DISCUSSION

The gas fraction at R_{500} is often cited to claim that clusters contain significantly fewer baryons than the universal baryon fraction and therefore exhibit a ‘missing baryon’ problem. Here we show, based purely on observational results, that the gas (and baryon) fraction increases substantially with radius beyond R_{500} ; the radius R_{500} cannot be used as a representative radius for comparisons with the global value. Using the observed gas and mass density profiles, we extrapolate the observed baryon fraction (gas and stars) as a function of radius from R_{500} to the virial radius. Since the gas-density is observed to decline more slowly with radius than the total mass, we find that the average baryon fraction increases with radius for clusters of all masses; it reaches the cosmic baryon fraction near the virial radius (R_{100}). This suggests that baryons are not missing in clusters, they are simply located in cluster outskirts.

Recent observations of the Sunyaev-Zeldovich (SZ) ef-

fect in 15 massive clusters using the South Pole Telescope [27] measure the gas density pressure profile in these clusters as a function of radius up to the virial radius (and beyond); they are well fit with a beta-model in the outer regions. The detection of the gas to these large radii, and their observed beta-model slope (when corrected for the temperature profile), are nicely consistent with our results and the conclusion that the baryons are out there between R_{500} and R_{vir} . Similarly, George et al. [36] use *Suzaku* X-ray observations to trace the gas density profile in the massive cluster PKS0745-191 up to the virial radius, observing the baryons at the cluster outskirts and measuring a shallow gas-density profile in these outer regions.

The gas density profile is observed to be even shallower in low-mass clusters than in massive clusters. This is consistent with the gas being heated via shocks and feedback from supernovae and AGN. This feedback will be more significant in low-mass systems when compared to the binding energy of the gas. If star formation is more efficient in groups than in clusters [e.g., 28], this will further increase the gas entropy in these systems, because the star formation removes the lowest-entropy gas from the intracluster medium, leaving behind gas with higher average entropy [37]. A higher stellar fraction also implies more supernovae/AGN activity per unit mass. This explains why, at R_{500} , groups have a lower baryon fraction than clusters. However, by the virial radius, we are able to account for all the baryons expected from the cosmic value.

A few comments on uncertainties are in order. First, the gas slopes we use from *ROSAT* observations [31, 32] are the best-fit slopes in the large radial range from R_{500} ($\sim 0.5R_{vir}$) to $\sim R_{vir}$. This is the average slope in these outer cluster regions which are relevant to our extrapolation. If we instead use the best measured gas-density slope at R_{500} [e.g., 8] and then steepen it slowly with radius similar to the steepening trend observed for the NFW profile (which steepens by 10% from R_{500} to R_{vir}), we find consistent results within the error-bars with the ones presented above.

The stellar fraction has been observed for a large number of clusters by Gonzalez et al. [30], who report a somewhat higher stellar fraction for low-mass clusters and a slightly lower stellar fraction for high-mass clusters than the observations by Giodini et al. [11] and Lin et al. [28]. The higher stellar fraction in groups [30] is likely due to a selection bias towards systems with dominant Brightest Cluster Galaxies in the small groups. Their observed trend of stellar fraction with mass is therefore somewhat steeper, $\log f^{stars} = (7.57 \pm 0.08) - (0.64 \pm 0.13) \log M_{500}$. Using this stellar fraction in our analysis does not change our result significantly; the baryon fraction at the virial radius decreases by $\approx 5\%$ for the most massive bin, and increases by $\approx 7\%$ for the lowest mass bin, but all are well within our $1\text{-}\sigma$ error bars.

We use the observed 10% contribution of the ICL to the stellar fraction [29]. If the ICL fraction changes at

the outer radii, it will not affect our results since the ICL contribution is only $\sim 0.2\text{--}0.4\%$ of total mass.

Similarly, we assume in our analysis that the stellar fraction does not change when extrapolated from R_{500} to R_{vir} , since no observations of the stellar fraction have been made beyond R_{500} . If the stellar mass fraction decreases somewhat with radius, then the baryon fraction will slightly decrease. If we assume, for example, a 20% decrease in stellar fraction from R_{500} to R_{vir} , we find that the baryon fraction is lowered by only 2% for the massive clusters and 8% for the low-mass groups (at R_{vir}); these values are within $1\text{-}\sigma$ of our baryon fraction results even for the lowest mass groups.

For the mass density profile, we use the mean observed value of the concentration parameter of the NFW profile, $c_{200} = 5$, as observed from weak lensing [38] for our mass range. As Mandelbaum et al. [38] discuss in their paper, this value is slightly lower than results from simulations and some previous studies. If c_{200} is larger than 5, the mass profile will be more concentrated, i.e., fall off even steeper with respect to the gas profile at the outer radii. This would cause the gas fraction to increase even more with radius. The effect is small, however, and a change of c_{200} to 7 induces a change in baryon fraction at the virial radius of $<5\%$. Earlier in this Section we discussed a scenario in which the gas density declines at the same trend as the NFW profile; in that scenario, the effects will nearly cancel out.

The observations presented above are consistent with an energy input in clusters that heats the intracluster gas and expands it to larger radii, where the missing baryons may be found. Hydrodynamic simulations of cluster formation which include the relevant physics are in qualitative good agreement (within $\sim 10\%$) with the picture presented here. Using simulations without cooling, star formation, or feedback, the baryon fraction is roughly constant, at 90% of the cosmic value, from R_{500} to R_{200} [40]. When these processes are included (with feedback coming from AGN), then the baryon fraction is found to be lower at R_{500} , but instead of being flat it increases with radius [41, 42]. Similar results, based on cluster energetics, are found in the models of Bode et al. [21]. Further improvements in models and simulations (including additional physical processes, sources of non-thermal pressure and possible non-equipartition effects) will be needed to provide precise comparisons with the observations.

IV. CONCLUSIONS

We investigate the ‘missing baryon’ problem in clusters of galaxies. Observations show that the baryon frac-

tion (gas plus stars) measured within a radius of R_{500} in groups and clusters is significantly below the cosmic value; this baryon discrepancy increases with decreasing cluster mass. This gives rise to the puzzle: Where are the missing baryons? Why are they missing? We show that the baryons may not be missing at all, but rather are spread out to larger radii, beyond R_{500} , and can be found in the cluster outskirts. Here we show that the radius R_{500} , which is typically used in observations, cannot serve as representative for the baryon fraction in groups and clusters. Based entirely on observations, we investigate the dependence of the baryon fraction on radius for clusters of different masses, from groups to rich clusters. We use the mean observed gas and mass density profiles in clusters to extrapolate the observed gas fraction as a function of radius from R_{500} to the virial radius. Since the gas-density profile is significantly shallower than the mass-density profile, the gas-fraction increases with radius; it increases more rapidly for groups than for rich clusters because of shallower gas-density slope in groups. We add the observed stellar fraction and the diffuse intracluster light to the gas fraction to obtain the total baryon fraction. We find that the average baryon fraction for all groups and clusters with $M_{500} \geq 5 \times 10^{13} h_{72}^{-1} M_{\odot}$ increases steadily with radius, reaching the cosmic value and becoming flat as a function of mass when measured within the virial radius (for the LCDM cosmology). This suggests that baryons are not missing in clusters, but are simply located in cluster outskirts. This picture is consistent with heating processes (such as shock-heating of the intracluster gas, as well as supernovae and AGN feedback) causing the gas to expand to the cluster outskirts. Upcoming observations in the X-rays and SZ should be able to detect these baryons.

Acknowledgments

B. R. owes a debt of gratitude to her research adviser, collaborator and friend Neta Bahcall for her judicious and delightfully rewarding stewardship of my senior thesis, which culminated in this paper. B. R. warmly thanks Princeton University for enabling this experience. The authors thank Rachel Mandelbaum, Greg Novak, David Spergel, Michael Strauss and Alexey Vikhlinin for their helpful comments. Computational work was performed at the TIGRESS high performance computer center at Princeton University, which is jointly supported by the Princeton Institute for Computational Science and Engineering and the Princeton University Office of Information Technology.

[1] Bahcall, N A (1988) Large-scale structure in the universe indicated by galaxy clusters. *Ann Rev Astron Astrophys*

- [2] Bahcall, N A, Ostriker, J P, Perlmutter, S, Steinhardt, P J (1999) The Cosmic Triangle: Revealing the State of the Universe *Science* 284:1481-1488
- [3] Rosati, P, Borgani, S, Norman, C (2002) The Evolution of X-ray Clusters of Galaxies. *Ann Rev Astron Astrophys* 40:539-577
- [4] Peebles, P J, Ratra, B (2003) The cosmological constant and dark energy. *Reviews of Modern Physics* 75:559-606
- [5] White, S D M, Navarro, J F, Evrard, A E, Frenk, C S (1993) The baryon content of galaxy clusters: a challenge to cosmological orthodoxy. *Nature* 366:429-433
- [6] Afshordi, N, Lin, Y-T, Nagai, D, Sanderson, A J R (2007) Missing thermal energy of the intracluster medium. *Mon Not R Astron Soc* 378:293-300
- [7] Umetsu, K, et al. (2009) Mass and Hot Baryons in Massive Galaxy Clusters from Subaru Weak-Lensing and AMiBA Sunyaev-Zeldovich Effect Observations. *Astrophys J* 694:1643-1663
- [8] Vikhlinin, A, et al. (2006) Chandra Sample of Nearby Relaxed Galaxy Clusters: Mass, Gas Fraction, and Mass-Temperature Relation. *Astrophys J* 640: 691-709
- [9] Arnaud, M, Pointecouteau, E, Pratt, G W (2007) Calibration of the galaxy cluster $M500 - YX$ relation with XMM-Newton. *Astron Astrophys* 474: L37-L40
- [10] Sun, M et al. (2009) Chandra Studies of the X-Ray Gas Properties of Galaxy Groups. *Astrophys J* 693:1142-1172
- [11] Giodini, S, et al. (2009) Chandra Studies of the X-Ray Gas Properties of Galaxy Groups. *Astrophys J* 703:982-993
- [12] Walker, T P, Steigman, G, Kang, H-S, Schramm, D M, Olive, K A (1991) Primordial nucleosynthesis redux. *Astrophys J* 376:51-69
- [13] Tytler, D, Fan, X-M, Burles, S (1996) Cosmological baryon density derived from the deuterium abundance at redshift $z = 3.57$. *Nature* 381:207-209
- [14] Jarosik, N, et al. (2010) Seven-Year Wilkinson Microwave Anisotropy Probe (WMAP) Observations: Sky Maps, Systematic Errors, and Basic Results. *Astrophys J Sup* submitted (arXiv:1001.4744)
- [15] Cavaliere, A, Fusco-Femiano, R (1978) The Distribution of Hot Gas in Clusters of Galaxies. *Astron Astrophys* 70:677+-
- [16] Metzler, C A, Evrard, A E (1994) A simulation of the intracluster medium with feedback from cluster galaxies. *Astrophys J* 437:564-583
- [17] Takizawa, M, Mineshige, S (1998) Evolution of X-Ray Clusters of Galaxies and Shock Heating of the Intracluster Medium. *Astrophys J* 499:82+-
- [18] Bialek, J J, Evrard, A E, Mohr, J J (2001) Effects of Preheating on X-Ray Scaling Relations in Galaxy Clusters. *Astrophys J* 555:597-612
- [19] Valdarnini, R (2003) Iron abundances and heating of the intracluster medium in hydrodynamical simulations of galaxy clusters. *Mon Not R Astron Soc* 339:1117-1134
- [20] McCarthy, I G, Bower, R G, Balogh, M L (2007) Revisiting the baryon fractions of galaxy clusters: a comparison with WMAP 3-yr results. *Mon Not R Astron Soc* 377:1457-1463
- [21] Bode, P, Ostriker, J P, Vikhlinin, A (2009) Exploring the Energetics of Intracluster Gas with a Simple and Accurate Model. *Astrophys J* 700:989-999
- [22] Bonamente, M, Lieu, R, Mittaz, J P D, Kaastra, J S, Nevalainen, J (2005) Thermal and Nonthermal Nature of the Soft Excess Emission from Sérsic 159-03 Observed with XMM-Newton. *Astrophys J* 629:192-203
- [23] Eke, V R, Cole, S, Frenk, C S (1996) Cluster evolution as a diagnostic for Omega. *Mon Not R Astron Soc* 282:263-280
- [24] Bryan, G L, Norman, M L (1998) Statistical Properties of X-Ray Clusters: Analytic and Numerical Comparisons. *Astrophys J* 495:80-
- [25] Navarro, J F, Frenk, C S, White, S D M (1996) The Structure of Cold Dark Matter Halos. *Astrophys J* 462:563+-
- [26] Fowler, J W et al. (2010) The Atacama Cosmology Telescope: A Measurement of the $600 < \ell < 8000$ Cosmic Microwave Background Power Spectrum at 148 GHz. *Astrophys J* submitted (arXiv:1001.2934)
- [27] Plagge, T, et al. (2010) Sunyaev-Zeldovich Cluster Profiles Measured with the South Pole Telescope. *Astrophys J* 716:1118-1135
- [28] Lin, Y-T, Mohr, J J, Stanford, S A (2003) Near-Infrared Properties of Galaxy Clusters: Luminosity as a Binding Mass Predictor and the State of Cluster Baryons. *Astrophys J* 591: 749-763
- [29] Zibetti, S (2008) Statistical Properties of the Intracluster Light from SDSS Image Stacking. *IAU Symposium* 244:176-185
- [30] Gonzalez, A H, Zaritsky, D, Zabludoff, A I (2007) A Census of Baryons in Galaxy Clusters and Groups. *Astrophys J* 666:147-155
- [31] Vikhlinin, A, Forman, W, Jones, C (1999) Outer Regions of the Cluster Gaseous Atmospheres. *Astrophys J* 525:47-57
- [32] Dai, X, Bregman, J N, Kochanek, C S, Rasia, E (2009) On the Baryon Fractions in Clusters and Groups of Galaxies. *Astrophys J* in press (arXiv:0911.2230)
- [33] Bautz, M W, et al (2009) Suzaku Observations of Abell 1795: Cluster Emission to r_{200} . *PASJ* 61:1117-
- [34] Pratt, G W, Arnaud, M (2003) Entropy scaling in galaxy clusters: Insights from an XMM-Newton observation of the poor cluster A1983. *Astron Astrophys* 408:1-16
- [35] Ettori, S, Balestra, I (2009) The outer regions of galaxy clusters: Chandra constraints on the X-ray surface brightness. *Astron Astrophys* 496:343-349
- [36] George, M R, Fabian, A C, Sanders, J S, Young, A J, Russell, H R (2009) X-ray observations of the galaxy cluster PKS0745-191: to the virial radius, and beyond. *Mon Not R Astron Soc* 395:657-666
- [37] Voit, G M, Bryan, G L (2001) On the Distribution of X-Ray Surface Brightness from Diffuse Gas. *Astrophys J* 551:L139-L142
- [38] Mandelbaum, R, Seljak, U, Hirata, C M (2008) A halo mass-concentration relation from weak lensing. *Journal of Cosmology and Astro-Particle Physics* 8:6
- [39] Sheldon, E S, et al (2009) Cross-correlation Weak Lensing of SDSS Galaxy Clusters. I. Measurements. *Astrophys J*, 703:2217-2231
- [40] Crain, R A et al. (2007) The baryon fraction of Λ CDM halos. *Mon Not R Astron Soc* 377:41-49
- [41] Sijacki, D, Pfrommer, C, Springel, V, Enßlin, T A (2008) Simulations of cosmic-ray feedback by active galactic nuclei in galaxy clusters. *Mon Not R Astron Soc* 387:1403-1415
- [42] Battaglia, N, Bond, J R, Pfrommer, C, Sievers, J L, Sijacki, D (2010) Simulations of the Sunyaev-Zeldovich Power Spectrum with AGN Feedback. *Astrophys J* submitted (arXiv:1003.4256B)

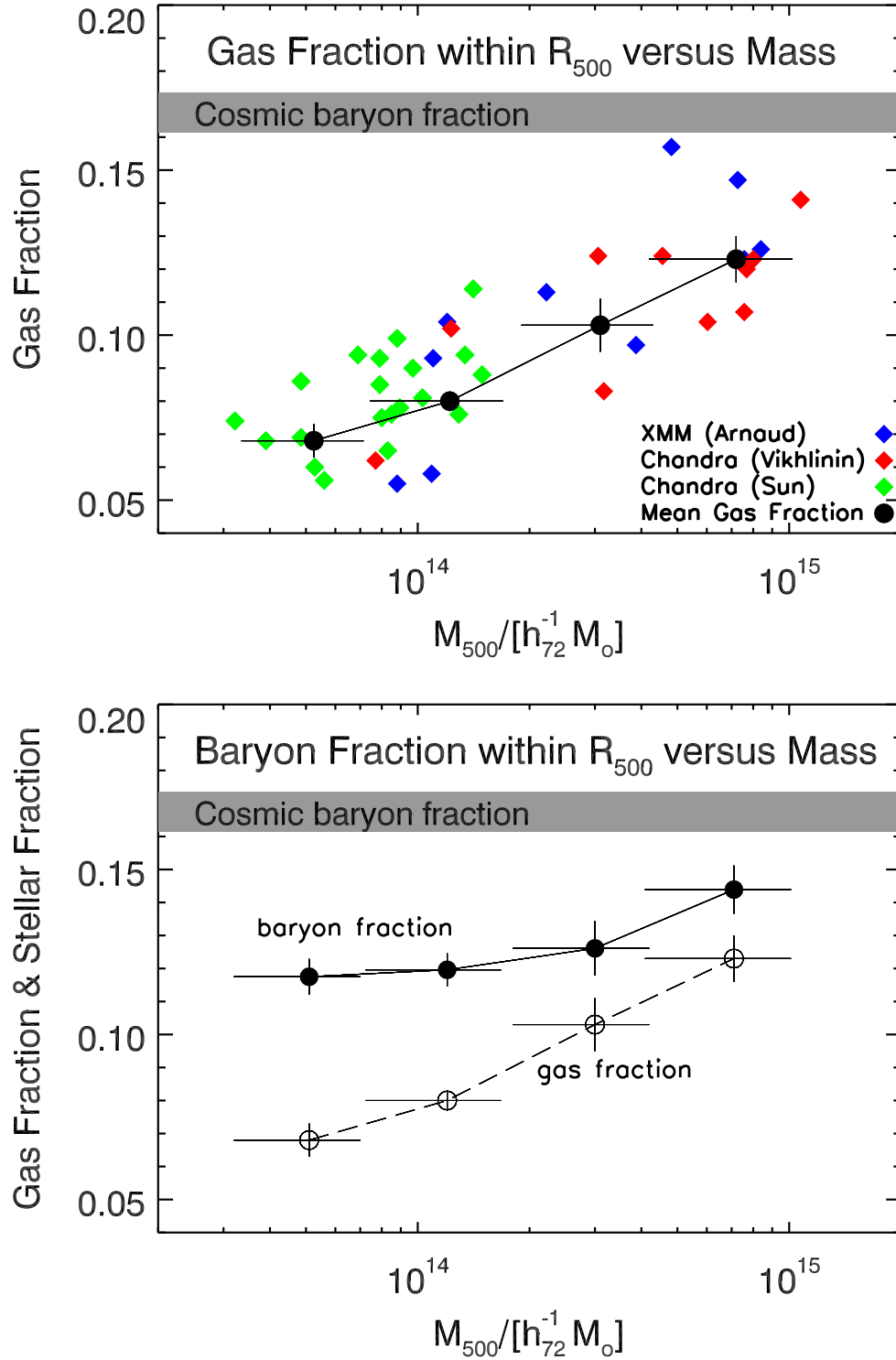


FIG. 1: The observed cluster gas and baryon fraction within R_{500} as a function of cluster mass, M_{500} . The observed cosmic baryon fraction is shown by the shaded band ($1\text{-}\sigma$; [14]). (a) Observed cluster gas fraction from *Chandra* and *XMM-Newton* within R_{500} [8–11]. The average for the four mass bins is shown by the filled circles. (b) Observed cluster gas and baryon fraction within R_{500} for the averages of the four mass bins. Error bars are $1\text{-}\sigma$ errors on the mean. Horizontal bars represent the mass range of each bin.

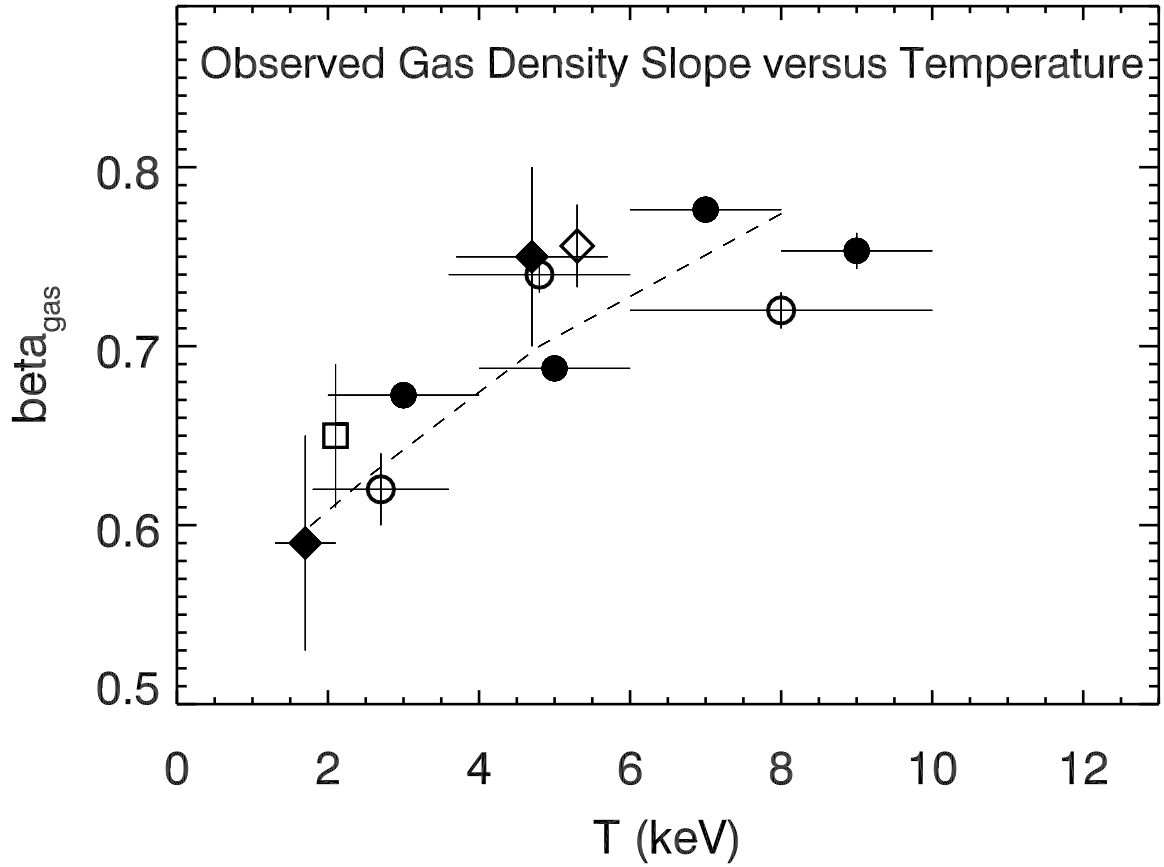


FIG. 2: Average observed gas density slope β_{gas} (where $\rho_{gas} \propto r^{-3\beta_{gas}}$) at $\geq R_{500}$ from *ROSAT*, *Chandra*, *XMM-Newton*, and *Suzaku* [8, 31–34] as a function of cluster temperature. Filled circles are bin-averages of 39 *ROSAT* clusters [31]; filled diamonds are *ROSAT* averages of hundreds of stacked optical clusters [32, their richness classes 0 and 1]; empty circles are bin-averages of 10 *Chandra* clusters [8]; empty diamond is *Suzaku* observation for Abell 1795 [33]; empty square is *XMM* observation for A1983 [34]. The dashed line illustrates the average trend of β_{gas} with T . Error bars are $1\text{-}\sigma$ errors on the mean. Horizontal bars represent the temperature bin size.

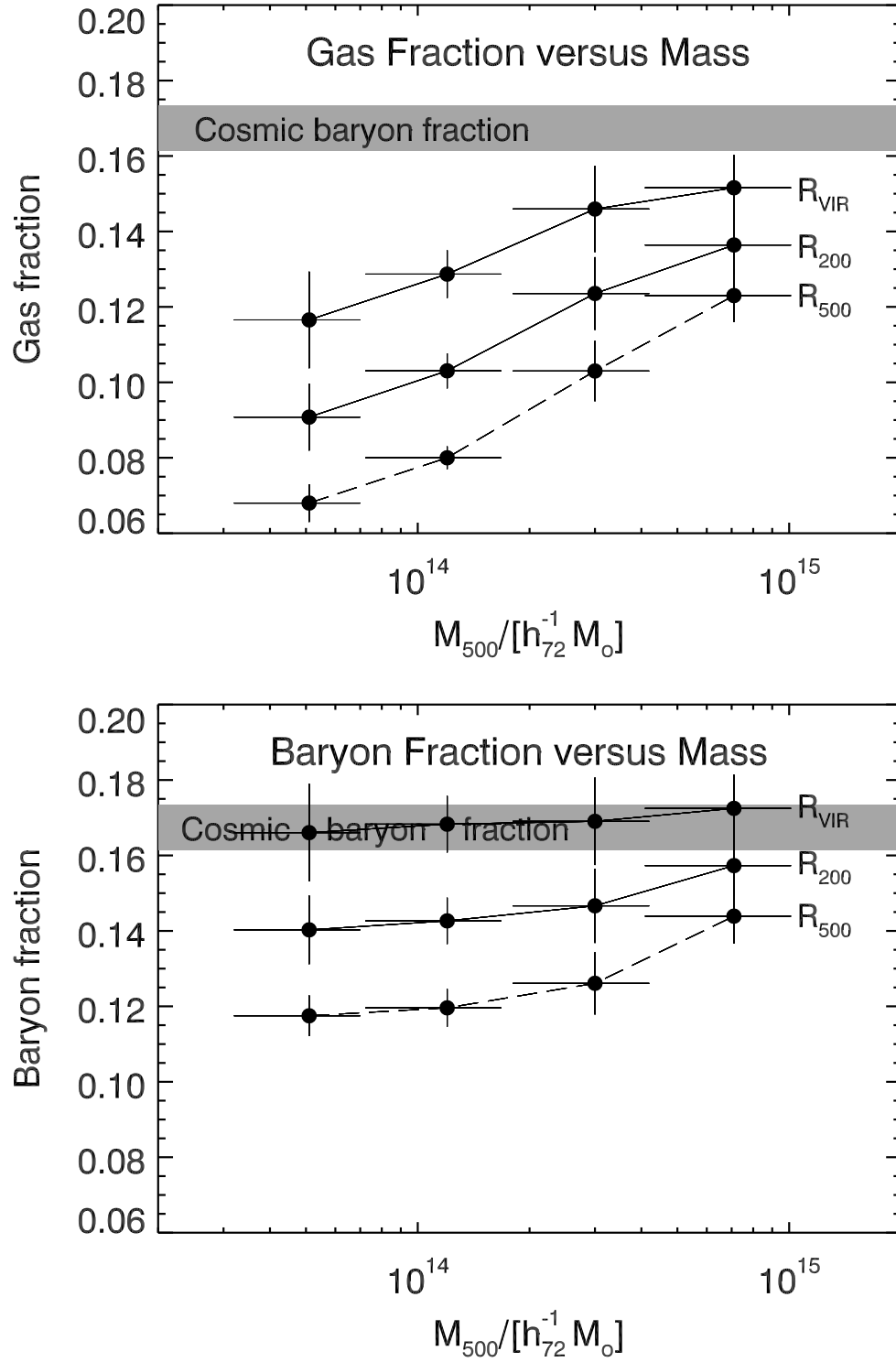


FIG. 3: Cluster gas and baryon fraction (3a and 3b, respectively) within R_{500} (observed), R_{200} and $R_{vir}(= R_{100})$ (extrapolated using observational data as discussed in the paper). The gas and baryon fractions are presented as a function of cluster mass for the four averaged binned samples. The error bars are the $1-\sigma$ error on the mean for each bin; horizontal bars represent the mass range of each bin. The observed cosmic baryon fraction is presented by the shaded band ($1-\sigma$).

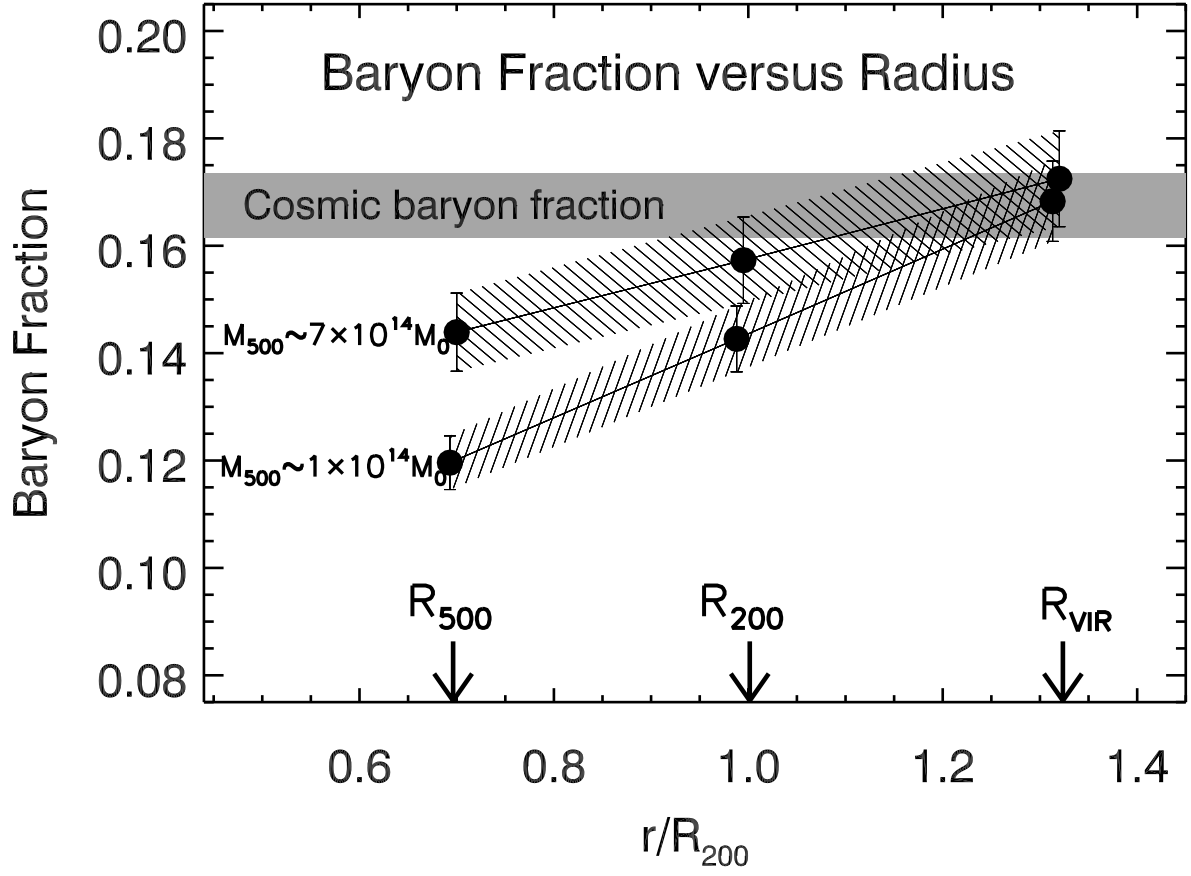


FIG. 4: The dependence of the baryon fraction on radius, from R_{500} to $R_{vir}(=R_{100})$, for two representative mass bins (bins 2 and 4; the others show a similar trend). The radius is presented in units of R_{200} . The slow but steady increase of the baryon fraction with radius is apparent, reaching the cosmic value near R_{vir} for all cluster masses. The error-bars are $1\text{-}\sigma$ errors on the mean.